DESY 05-040 ISSN 0418-9833
March 2005

Measurement of Charm and Beauty Photoproduction at HERA using $D^*\mu$ Correlations

H1 Collaboration

Abstract

A measurement of charm and beauty photoproduction at the electron proton collider HERA is presented based on the simultaneous detection of a $D^{*\pm}$ meson and a muon. The correlation between the D^* meson and the muon serves to separate the charm and beauty contributions and the analysis provides comparable sensitivity to both. The total and differential experimental cross sections are compared to LO and NLO QCD calculations. The measured charm cross section is in good agreement with QCD predictions including higher order effects while the beauty cross section is higher.

To be submitted to Phys. Lett. B

A. Aktas[10], V. Andreev[26], T. Anthonis[4], S. Aplin[10], A. Asmone[34], A. Astvatsatourov[4],
A. Babaev[25], S. Backovic[31], J. Bähr[39], A. Baghdasaryan[38], P. Baranov[26], E. Barrelet[30],
W. Bartel[10], S. Baudrand[28], S. Baumgartner[40], J. Becker[41], M. Beckingham[10], O. Behnke[13],
O. Behrendt[7], A. Belousov[26], Ch. Berger[1], N. Berger[40], J.C. Bizot[28], M.-O. Boenig[7],
V. Boudry[29], J. Bracinik[27], G. Brandt[13], V. Brisson[28], D.P. Brown[10], D. Bruncko[16],
F.W. Büsser[11], A. Bunyatyan[12,38], G. Buschhorn[27], L. Bystritskaya[25], A.J. Campbell[10],
S. Caron[1], F. Cassol-Brunner[22], K. Cerny[33], V. Cerny[16,47], V. Chekelian[27], J.G. Contreras[23],
J.A. Coughlan[5], B.E. Cox[21], G. Cozzika[9], J. Cvach[32], J.B. Dainton[18], W.D. Dau[15],
K. Daum[37,43], B. Delcourt[28], R. Demirchyan[38], A. De Roeck[10,45], K. Desch[11], E.A. De Wolf[4],
C. Diaconu[22], V. Dodonov[12], A. Dubak[31,46], G. Eckerlin[10], V. Efremenko[25], S. Egli[36],
R. Eichler[36], F. Eisele[13], M. Ellerbrock[13], E. Elsen[10], W. Erdmann[40], S. Essenov[25],
A. Falkewicz[6], P.J.W. Faulkner[3], L. Favart[4], A. Fedotov[25], R. Felst[10], J. Ferencei[10], L. Finke[11],
M. Fleischer[10], P. Fleischmann[10], Y.H. Fleming[10], G. Flucke[10], A. Fomenko[26], I. Foresti[41],
J. Formánek[33], G. Franke[10], G. Frising[1], T. Frisson[29], E. Gabathuler[18], E. Garutti[10],
J. Gayler[10], R. Gerhards[10,†], C. Gerlich[13], S. Ghazaryan[38], S. Ginzburgskaya[25], A. Glazov[10],
I. Glushkov[39], L. Goerlich[6], M. Goettlich[10], N. Gogitidze[26], S. Gorbounov[39], C. Goyon[22],
C. Grab[40], T. Greenshaw[18], M. Gregori[19], G. Grindhammer[27], C. Gwilliam[21], D. Haidt[10],
L. Hajduk[6], J. Haller[13], M. Hansson[20], G. Heinzelmann[11], R.C.W. Henderson[17],
H. Henschel[39], O. Henshaw[3], G. Herrera[24], M. Hildebrandt[36], K.H. Hiller[39], D. Hoffmann[22],
R. Horisberger[36], A. Hovhannisyan[38], M. Ibbotson[21], M. Ismail[21], M. Jacquet[28],
L. Janauschek[27], X. Janssen[10], V. Jemanov[11], L. Jönsson[20], D.P. Johnson[4], H. Jung[20,10],
M. Kapichine[8], M. Karlsson[20], J. Katzy[10], N. Keller[41], I.R. Kenyon[3], C. Kiesling[27],
M. Klein[39], C. Kleinwort[10], T. Klimkovich[10], T. Kluge[10], G. Knies[10], A. Knutsson[20],
V. Korbel[10], P. Kostka[39], R. Koutouev[12], K. Krastev[35], J. Kretzschmar[39], A. Kropivnitskaya[25],
K. Krüger[14], J. Kückens[10], M.P.J. Landon[19], W. Lange[39], T. Laštovička[39,33], P. Laycock[18],
A. Lebedev[26], B. Leißner[1], V. Lendermann[14], S. Levonian[10], L. Lindfeld[41], K. Lipka[39],
B. List[40], E. Lobodzinska[39,6], N. Loktionova[26], R. Lopez-Fernandez[10], V. Lubimov[25],
A.-I. Lucaci-Timoce[10], H. Lueders[11], D. Lüke[7,10], T. Lux[11], L. Lytkin[12], A. Makankine[8],
N. Malden[21], E. Malinovski[26], S. Mangano[40], P. Marage[4], R. Marshall[21], M. Martisikova[10],
H.-U. Martyn[1], S.J. Maxfield[18], D. Meer[40], A. Mehta[18], K. Meier[14], A.B. Meyer[11],
H. Meyer[37], J. Meyer[10], S. Mikocki[6], I. Milcewicz-Mika[6], D. Milstead[18], A. Mohamed[18],
F. Moreau[29], A. Morozov[8], J.V. Morris[5], M.U. Mozer[13], K. Müller[41], P. Murín[16,44],
K. Nankov[35], B. Naroska[11], J. Naumann[7], Th. Naumann[39], P.R. Newman[3], C. Niebuhr[10],
A. Nikiforov[27], D. Nikitin[8], G. Nowak[6], M. Nozicka[33], R. Oganezov[38], B. Olivier[3],
J.E. Olsson[10], S. Osman[20], D. Ozerov[25], V. Palichik[8], T. Papadopoulou[10], C. Pascaud[28],
G.D. Patel[18], M. Peez[29], E. Perez[9], D. Perez-Astudillo[23], A. Perieanu[10], A. Petrukhin[25],
D. Pitzl[10], R. Plačakytė[27], B. Portheault[28], B. Povh[12], P. Prideaux[18], N. Raicevic[31],
P. Reimer[32], A. Rimmer[18], C. Risler[10], E. Rizvi[3], P. Robmann[41], B. Roland[4], R. Roosen[4],
A. Rostovtsev[25], Z. Rurikova[27], S. Rusakov[26], F. Salvaire[11], D.P.C. Sankey[5], E. Sauvan[22],
S. Schätzel[13], F.-P. Schilling[10], S. Schmidt[10], S. Schmitt[41], C. Schmitz[41], L. Schoeffel[9],
A. Schöning[40], V. Schröder[10], H.-C. Schultz-Coulon[14], C. Schwanenberger[10], K. Sedlák[32],
F. Sefkow[10], I. Sheviakov[26], L.N. Shtarkov[26], Y. Sirois[29], T. Sloan[17], P. Smirnov[26],
Y. Soloviev[26], D. South[10], V. Spaskov[8], A. Specka[29], B. Stella[34], J. Stiewe[14], I. Strauch[10],
U. Straumann[41], V. Tchoulakov[8], G. Thompson[19], P.D. Thompson[3], F. Tomasz[14],
D. Traynor[19], P. Truöl[41], I. Tsakov[35], G. Tsipolitis[10,42], I. Tsurin[10], J. Turnau[6],
E. Tzamariudaki[27], M. Urban[41], A. Usik[26], D. Utkin[25], S. Valkár[33], A. Valkárová[33],

C. Vallée[22], P. Van Mechelen[4], N. Van Remortel[4], A. Vargas Trevino[7], Y. Vazdik[26], C. Veelken[18], A. Vest[1], S. Vinokurova[10], V. Volchinski[38], B. Vujicic[27], K. Wacker[7], J. Wagner[10], G. Weber[11], R. Weber[40], D. Wegener[7], C. Werner[13], N. Werner[41], M. Wessels[10], B. Wessling[10], C. Wigmore[3], G.-G. Winter[10], Ch. Wissing[7], R. Wolf[13], E. Wünsch[10], S. Xella[41], W. Yan[10], V. Yeganov[38], J. Žáček[33], J. Zálešák[32], Z. Zhang[28], A. Zhelezov[25], A. Zhokin[25], J. Zimmermann[27], H. Zohrabyan[38], and F. Zomer[28]

[1] *I. Physikalisches Institut der RWTH, Aachen, Germany*[a]
[2] *III. Physikalisches Institut der RWTH, Aachen, Germany*[a]
[3] *School of Physics and Astronomy, University of Birmingham, Birmingham, UK*[b]
[4] *Inter-University Institute for High Energies ULB-VUB, Brussels; Universiteit Antwerpen, Antwerpen; Belgium*[c]
[5] *Rutherford Appleton Laboratory, Chilton, Didcot, UK*[b]
[6] *Institute for Nuclear Physics, Cracow, Poland*[d]
[7] *Institut für Physik, Universität Dortmund, Dortmund, Germany*[a]
[8] *Joint Institute for Nuclear Research, Dubna, Russia*
[9] *CEA, DSM/DAPNIA, CE-Saclay, Gif-sur-Yvette, France*
[10] *DESY, Hamburg, Germany*
[11] *Institut für Experimentalphysik, Universität Hamburg, Hamburg, Germany*[a]
[12] *Max-Planck-Institut für Kernphysik, Heidelberg, Germany*
[13] *Physikalisches Institut, Universität Heidelberg, Heidelberg, Germany*[a]
[14] *Kirchhoff-Institut für Physik, Universität Heidelberg, Heidelberg, Germany*[a]
[15] *Institut für experimentelle und Angewandte Physik, Universität Kiel, Kiel, Germany*
[16] *Institute of Experimental Physics, Slovak Academy of Sciences, Košice, Slovak Republic*[f]
[17] *Department of Physics, University of Lancaster, Lancaster, UK*[b]
[18] *Department of Physics, University of Liverpool, Liverpool, UK*[b]
[19] *Queen Mary and Westfield College, London, UK*[b]
[20] *Physics Department, University of Lund, Lund, Sweden*[g]
[21] *Physics Department, University of Manchester, Manchester, UK*[b]
[22] *CPPM, CNRS/IN2P3 - Univ Mediterranee, Marseille - France*
[23] *Departamento de Fisica Aplicada, CINVESTAV, Mérida, Yucatán, México*[k]
[24] *Departamento de Fisica, CINVESTAV, México*[k]
[25] *Institute for Theoretical and Experimental Physics, Moscow, Russia*[l]
[26] *Lebedev Physical Institute, Moscow, Russia*[e]
[27] *Max-Planck-Institut für Physik, München, Germany*
[28] *LAL, Université de Paris-Sud, IN2P3-CNRS, Orsay, France*
[29] *LLR, Ecole Polytechnique, IN2P3-CNRS, Palaiseau, France*
[30] *LPNHE, Universités Paris VI and VII, IN2P3-CNRS, Paris, France*
[31] *Faculty of Science, University of Montenegro, Podgorica, Serbia and Montenegro*
[32] *Institute of Physics, Academy of Sciences of the Czech Republic, Praha, Czech Republic*[e,i]
[33] *Faculty of Mathematics and Physics, Charles University, Praha, Czech Republic*[e,i]
[34] *Dipartimento di Fisica Università di Roma Tre and INFN Roma 3, Roma, Italy*
[35] *Institute for Nuclear Research and Nuclear Energy , Sofia,Bulgaria*
[36] *Paul Scherrer Institut, Villingen, Switzerland*
[37] *Fachbereich C, Universität Wuppertal, Wuppertal, Germany*
[38] *Yerevan Physics Institute, Yerevan, Armenia*

[39] *DESY, Zeuthen, Germany*
[40] *Institut für Teilchenphysik, ETH, Zürich, Switzerland*[j]
[41] *Physik-Institut der Universität Zürich, Zürich, Switzerland*[j]

[42] *Also at Physics Department, National Technical University, Zografou Campus, GR-15773 Athens, Greece*
[43] *Also at Rechenzentrum, Universität Wuppertal, Wuppertal, Germany*
[44] *Also at University of P.J. Šafárik, Košice, Slovak Republic*
[45] *Also at CERN, Geneva, Switzerland*
[46] *Also at Max-Planck-Institut für Physik, München, Germany*
[47] *Also at Comenius University, Bratislava, Slovak Republic*

[†] *Deceased*

[a] *Supported by the Bundesministerium für Bildung und Forschung, FRG, under contract numbers 05 H1 1GUA /1, 05 H1 1PAA /1, 05 H1 1PAB /9, 05 H1 1PEA /6, 05 H1 1VHA /7 and 05 H1 1VHB /5*
[b] *Supported by the UK Particle Physics and Astronomy Research Council, and formerly by the UK Science and Engineering Research Council*
[c] *Supported by FNRS-FWO-Vlaanderen, IISN-IIKW and IWT and by Interuniversity Attraction Poles Programme, Belgian Science Policy*
[d] *Partially Supported by the Polish State Committee for Scientific Research, SPUB/DESY/P003/DZ 118/2003/2005*
[e] *Supported by the Deutsche Forschungsgemeinschaft*
[f] *Supported by VEGA SR grant no. 2/4067/ 24*
[g] *Supported by the Swedish Natural Science Research Council*
[i] *Supported by the Ministry of Education of the Czech Republic under the projects INGO-LA116/2000 and LN00A006, by GAUK grant no 173/2000*
[j] *Supported by the Swiss National Science Foundation*
[k] *Supported by CONACYT, México, grant 400073-F*
[l] *Partially Supported by Russian Foundation for Basic Research, grant no. 00-15-96584*

1 Introduction

At the electron proton collider HERA, heavy quarks are predominantly produced via photon-gluon fusion, $\gamma g \to c\bar{c}$ or $b\bar{b}$, where the photon is emitted from the incoming lepton and the gluon from the proton. The production cross sections are largest for photoproduction, i.e. for photons with virtuality $Q^2 \simeq 0$. The light quarks u, d and s are produced much more copiously than c and b, and beauty production is suppressed by a factor of approximately 200 compared to charm. Charm and beauty measurements performed at HERA so far relied on the tagging of only one heavy quark in each event. While the charm measurements [1–11] were mostly based on the reconstruction of D mesons, the beauty measurements [12–17] used semi-leptonic decays or lifetime signatures or both. Here an analysis is presented, where in a large fraction of events *both* heavy quarks are tagged using a $D^{*\pm}$ meson and a muon as signatures. The correlations between the direction of the muon with respect to the $D^{*\pm}$ and their electric charges are used to separate charm and beauty contributions. Total cross sections are measured separately for the processes $ep \to ec\bar{c}X \to eD^*\mu X'$ and $ep \to eb\bar{b}X \to eD^*\mu X'$ in the visible kinematic region, while differential cross sections are derived for combined samples of $c\bar{c}$ and $b\bar{b}$ events. The measurements, which are based on an integrated luminosity of $\mathcal{L} = 89$ pb^{-1}, are compared to leading order (LO) and next-to-leading order (NLO) perturbative QCD (pQCD) calculations.

This measurement extends to significantly lower centre-of-mass energies of the $b\bar{b}$ system than previous measurements of beauty cross sections at HERA. The simultaneous detection of the D^* meson and the muon makes possible new tests of higher order QCD effects. For instance, in the photon-gluon rest frame the angle between the heavy quarks is $180°$ at leading order, but at next-to-leading order it can differ significantly from this value due to hard gluon radiation. Furthermore, the $D^*\mu$ pair is expected to be sensitive to a possible transverse momentum k_t of the gluons entering the quark pair production process.

2 Separation of Charm and Beauty

The separation of charm and beauty contributions exploits the charge and azimuthal angle[1] correlations of the D^* meson and the muon. The azimuthal angle difference $\Delta\Phi$ between the D^* and the muon and their respective electric charges $Q(D^*)$ and $Q(\mu)$ are used to define four 'correlation regions' I–IV. For $Q(D^*) = Q(\mu)$ regions I and II cover $\Delta\Phi < 90°$ and $\Delta\Phi > 90°$, respectively. Regions III and IV are defined correspondingly for $Q(D^*) \neq Q(\mu)$.

The four regions are populated differently by charm and beauty events as is illustrated in figure 1. Neglecting any transverse momenta of the photon and the gluon, the fusion process $\gamma g \to c\bar{c}$ or $b\bar{b}$ leads to a back-to-back configuration of the two heavy quarks. Approximating the directions of the $D^{*\pm}$ meson and the muon with those of the quark and antiquark and selecting opposite charges, $c\bar{c}$ pairs populate correlation region IV. In contrast, beauty events populate regions II, III and IV, depending on whether the muon originates from the same b quark as the D^* or from the opposite $\bar{b}$. If the muon originates from the same b quark as the D^* meson,

[1] The coordinate system is defined with the z-axis pointing in the proton beam direction and x (y) pointing in the horizontal (vertical) direction. The azimuthal angle Φ is measured in the x-y plane and the polar angle θ with respect to the z direction.

the events lie in region III. For muons coming from the $\bar{b}$ opposite to the D^* meson, the direct decay populates region II, while the cascade process $\bar{b} \rightarrow \bar{c} \rightarrow \mu$ populates region IV. Region IV hence receives contributions from both $c\bar{c}$ and $b\bar{b}$ events and region I stays empty.

The azimuthal angle correlations are smeared by fragmentation and semileptonic decay processes and by higher order QCD effects such as gluon radiation and any initial transverse momentum of the gluon. Processes such as heavy quark decays via τ leptons conserve the charge correlation, which is not the case for B^0-$\bar{B}^0$ mixing and e.g. the decays $b \rightarrow cW^-; W^- \rightarrow \bar{c}s$. According to the PYTHIA Monte Carlo simulation [18], which takes into account these smearing effects, the relative population of the four regions is as given by the numbers in figure 1. These numbers apply in the analysed kinematic region defined in section 4.1 and do not include detector effects. Since the population of the four correlation regions is very different for $b\bar{b}$ and $c\bar{c}$, it can be used for the separation of these two components.

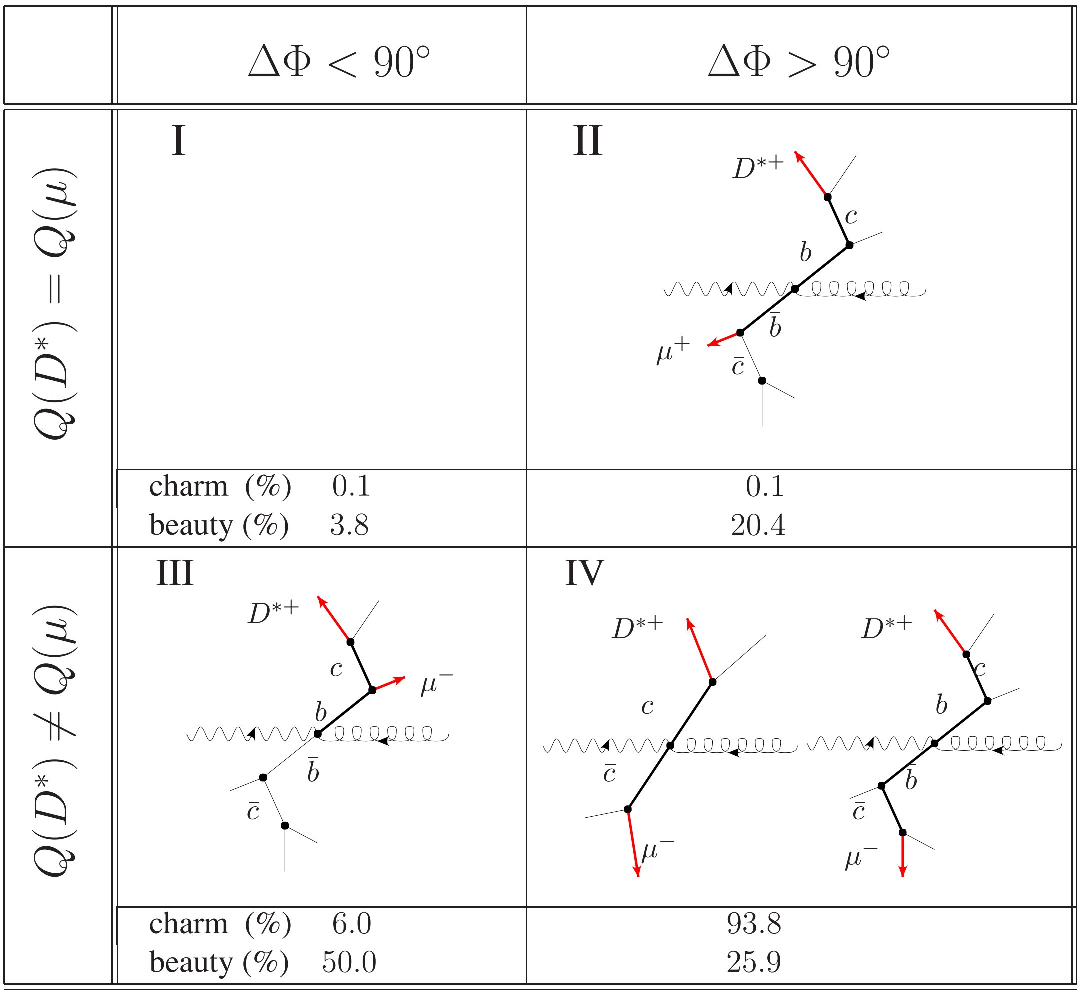

Figure 1: *Definition of the correlation regions in terms of $\Delta\Phi$ and the relative charges of the D^* meson and the muon. The sketches illustrate these correlations in $c\bar{c}$ and $b\bar{b}$ quark decays to $D^*\mu$. The numbers represent the relative distribution over the four correlation regions of charm and beauty events that satisfy the cuts given in section 4.1, as obtained from the PYTHIA simulation without detector effects.*

3 QCD Calculations and Monte Carlo Simulations

The Monte Carlo simulations PYTHIA [18] and CASCADE [19] are used for the description of the signal and background distributions in the separation of charm and beauty, for the determination of efficiencies and acceptances and for systematic studies. Their predictions are also compared with the measured cross sections. In PYTHIA and CASCADE leading order matrix elements which take into account the mass of the heavy quark are implemented and parton showers in the initial and final state are included to approximate higher orders (LO-ME+PS). The parton evolution in PYTHIA uses the DGLAP equations [20]. In addition to the direct process, a resolved photon component is generated in PYTHIA where the photon fluctuates into a hadronic state acting as a source of partons, one of which participates in the hard interaction. This component is dominated by heavy flavour excitation processes [21], where the heavy quark is a constituent of the resolved photon. In the PYTHIA calculation of heavy flavour excitation, in which quark masses are neglected, the contribution of excitation to the total charm cross section in the analysed kinematic region is found to be 41%, while it is 23% for beauty. In comparison to this component the contribution of the resolved component due to light quarks or gluons in the photon can be neglected in the present analysis, as can the heavy flavour component of the proton.

CASCADE contains an implementation of the CCFM [22] evolution equation for the initial state parton shower. The $\gamma g \rightarrow c\bar{c}$ or $b\bar{b}$ is implemented using off-shell matrix elements convoluted with k_t unintegrated proton parton distributions. PYTHIA and CASCADE use the JETSET program as implemented in PYTHIA for the hadronisation (via the Peterson fragmentation function [23]) and for the decay of beauty and charm quarks. In order to correct for detector effects, the generated events are passed through a detailed simulation of the detector response based on the GEANT program [24] and the same reconstruction software as used for the data.

The measured cross sections are also compared with NLO pQCD calculations in the massive scheme [25] using the program FMNR [26]. These calculations are expected to give reliable results in the kinematic region considered here, where the transverse momentum of the heavy quark is of the same order of magnitude as its mass. The calculations are available for both the direct and resolved photon processes. However, in contrast to the PYTHIA program, heavy flavour excitation is not explicitly included in the resolved part of the FMNR program. The contributions of the resolved light quark and gluon components are found to be small in FMNR ($< 3\%$ for charm and $< 6\%$ for beauty in the analysed kinematic region) and are neglected.

The original FMNR program is extended to include the effects of the hadronisation of c and b quarks and their semileptonic decays in order to make comparisons with the measured cross sections in the experimentally accessible kinematical region. The heavy quark is 'hadronised' by rescaling the three momentum of the quark using the Peterson fragmentation function. For the decay into muons the momentum spectrum is implemented as obtained from JETSET. In the case of beauty quarks, the direct decays of b-flavoured hadrons into muons are taken into account as are the decays via a charm quark, $b \rightarrow c \rightarrow \mu$. When the D^* meson and the muon originate from the same quark, the angular and momentum correlations are implemented as in JETSET. The measured fragmentation fractions [27, 28] for c and b quarks given in table 1 are used for the calculation of the cross sections. The important parameters of the pQCD programs used in this analysis are summarised in table 2.

Fragmentation Fractions [%]			
$c \to D^*$	23.5 ± 0.7	$c \to \mu$	9.8 ± 0.5
$b \to D^*$	17.3 ± 1.6	$b \to \mu$	10.95 ± 0.27
$b \to c \to \mu$	10.03 ± 0.64	$b \to D^*\mu$	2.75 ± 0.19

Table 1: *Fragmentation fractions [27, 28] used in the QCD calculations of the cross sections. The $b \to c \to \mu$ fraction also contains the $b \to c\bar{c}s$ decay and the τ contributions.*

	PYTHIA	**CASCADE**	**FMNR (NLO)**	**FMNR (LO)**
Version	6.1	1.2007		
Proton PDF	CTEQ5L [30]	J2003 [19]	CTEQ5M [30]	CTEQ5L [30]
Photon PDF	GRV-G LO [31]	–	GRV-G HO [31]	GRV-G LO [31]
Renorm. scale μ_r^2	$m_q^2 + p_{Tq}^2$	$4m_q^2 + p_{Tq}^2$	$m_q^2 + p_{Tq\bar{q}}^2$	
Factor. scale μ_f^2	$m_q^2 + p_{Tq}^2$	$\hat{s} + Q_T^2$	$m_b^2 + p_{Tb\bar{b}}^2$, $4(m_c^2 + p_{Tc\bar{c}}^2)$	
m_b [GeV]	4.8	4.8	4.75	
m_c [GeV]	1.5	1.5	1.5	
Peterson ϵ_b	0.008	0.008	0.0033 (0.42 for $b \to D^*$)	0.0069
Peterson ϵ_c	0.078	0.078	0.035	0.058

Table 2: *Parameters used in the Monte Carlo and NLO programs. The FMNR calculations are performed in the $\overline{MS}$ scheme using the default values of Λ_{QCD} for the parton density functions. μ_r and μ_f denote the renormalisation and factorisation scales, $p_{Tq\bar{q}}^2$ the average of the squares of the transverse momenta of the two heavy quarks, m_q the heavy quark masses, $\hat{s}$ the centre-of-mass energy squared, Q_T^2 the transverse momentum squared of the heavy quark system, p_{Tq} the transverse momentum of a heavy quark and ϵ_q the Peterson fragmentation parameters [29]. For the B^0-$\bar{B}^0$ mixing values of $x_d \equiv \Delta m_{B_d^0}/\Gamma_{B_d^0} = 0.73$ and $x_s = 18$ [28] are used.*

4 Data Analysis

The data were collected with the H1 detector [32, 33] at HERA during the years 1997 to 2000 and correspond to an integrated luminosity of $\mathcal{L} = 89$ pb^{-1}. The largest part of the luminosity (80%) was collected at a centre-of-mass energy of $\sqrt{s} \approx 320\,$GeV, the beam energies being 27.6 GeV and 920 GeV for electrons[2] and protons, respectively. The remaining 20% of the luminosity was taken at $\sqrt{s} \approx 300\,$GeV (proton energy 820 GeV).

4.1 Event Selection

A detailed account of this analysis can be found in [34]. Events with at least one reconstructed D^* and at least one muon are selected; multiple D^* or muon combinations are treated as separate events. The D^* is reconstructed via the decay channel[3] $D^{*+} \to D^0\pi_s^+ \to K^-\pi^+\pi_s^+$ (branching ratio $(2.59 \pm 0.06)\%$ [28]), where π_s refers to the low momentum π in the decay. The decay

[2]HERA has been operated with electron and positron beams. These periods will not be distinguished in this analysis.

[3]Charge conjugate states are always implicitly included.

particles of the D^* meson are reconstructed in the central tracking detector ($20^\circ \leq \theta \leq 160^\circ$) without particle identification. Muons are identified by reconstructing track segments in the instrumented iron return yoke of the solenoidal magnet. These are linked to tracks in the central tracking detector. In order to ensure good detector acceptance, cuts on the transverse momentum p_T with respect to the proton direction and the pseudorapidity $\eta = -\ln\ \tan(\theta/2)$ are applied for the D^* meson and the muon in the laboratory frame (see table 3).

Photoproduction events are selected by demanding the absence of any signals for the scattered electron, restricting the accepted range of negative four-momentum transfer squared Q^2 to be below 1 GeV^2. A cut on the inelasticity $0.05 < y < 0.75$ is applied, where $y = P \cdot q / P \cdot k$ (q, k and P are the four vectors of the exchanged photon, incoming electron and proton, respectively). The variable y is reconstructed from the measured hadronic final state using the Jacquet-Blondel method [35]. The events are triggered by fast signals from the central tracking and muon detectors. The analysed 'visible' kinematic region of the measurement is defined in table 3.

Selection of $D^* \to D^0\pi_s \to K\pi\pi_s$	$p_T(K), p_T(\pi) > 0.4$ GeV $p_T(\pi_s) > 0.12$ GeV $\mid m_{K\pi} - m_{D^0} \mid < 0.080$ GeV $\Delta M = m_{K\pi\pi_s} - m_{K\pi} < 0.1685$ GeV
Visible kinematic region	$p_T(D^*) > 1.5$ GeV $\mid \eta(D^*) \mid < 1.5$ $p(\mu) > 2$ GeV $\mid \eta(\mu) \mid < 1.735$ $0.05 < y < 0.75$ $Q^2 < 1$ GeV^2

Table 3: *The D^*selection cuts and definition of the visible kinematic region.*

4.2 Fit Procedure

The D^* yield is measured using the ΔM technique [36], where $\Delta M = m_{K\pi\pi_s} - m_{K\pi}$ is the difference of the invariant masses of the $K\pi\pi_s$ and the $K\pi$ systems. Figure 2a shows the ΔM distribution for the selected $D^*\mu$ sample separately for the 'right' ($K^-\pi^+\pi_s^+$) and 'wrong' ($K^-\pi^-\pi_s^+$) charge combinations. The wrong charge distribution is normalised to the right charge distribution in the range $0.155 \leq \Delta M \leq 0.1685$ GeV. The number of signal events is extracted from a fit to the ΔM distribution using a Gaussian function for the signal and a parameterisation of the background[4]. The parameters of the background function are determined from right and normalised wrong charge combinations. The result of this fit for the total signal is also shown in figure 2a.

The total number of $D^*\mu$ events obtained from the fit is $N_{D^*\mu} = 151 \pm 22$. This number still contains a contribution from 'fake muons', i.e. from hadrons misidentified as muons and

[4]The functional form used is $c_1\,(\Delta M - m_\pi)^{c_2}\,(1 - c_3\,(\Delta M)^2)$ where c_i are fit parameters.

muons from the decay of light mesons. The fake muon background contributes about 37% in charm and 5% in beauty initiated events according to the respective PYTHIA Monte Carlo simulations, which give an adequate description of the data.

In figure 2b–e, the ΔM distributions of the selected $D^*\mu$ events are shown separately for the four correlation regions defined in section 2. Clear peaks due to D^* mesons are observed in regions II-IV, whereas region I shows little or no signal, consistent with the expectation.

The charm and beauty contributions in the data are determined by performing a simultaneous likelihood fit of the ΔM distributions in the four correlation regions. In the following, this fit will be referred to as a 'two-dimensional fit', in order to distinguish the results from the separate one-dimensional fits of ΔM in each correlation region.

In this two-dimensional fit, in addition to the $D^*\mu$ contribution from $b\bar{b}$ and $c\bar{c}$, the fake muon background and the combinatorial background under the ΔM peaks have to be considered. The position and width of the ΔM peak corresponding to the D^* signal as well as the parameters describing the shape of the combinatorial background are fixed to the values obtained from the one-dimensional ΔM fit to the total sample (figure 2a). The normalisation of the combinatorial background is fitted using right and wrong charge combinations in each region separately. The relative distributions of signal events from charm and beauty between the correlation regions as well as the fractions of fake muon background in each region predicted by the PYTHIA Monte Carlo simulations are used as input for the fit. In total there are six free fit parameters, the total numbers of $D^*\mu$ events from $b\bar{b}$ and $c\bar{c}$ quark pairs, N_b and N_c, and four parameters for the combinatorial background, one in each correlation region.

5 Results

The result of the two-dimensional fit is shown together with the data in figures 2b–e. The data are described well and the quality of the fit is good ($\chi^2 = 145.5$ for 154 $d.o.f.$). In figure 3, the numbers of D^* signal events from the two-dimensional fit in the four correlation regions are compared to the results of one-dimensional fits of the ΔM distributions performed in each correlation region separately. The agreement is very good. The distribution of the contributing processes as obtained from the two-dimensional fit is also shown in figure 3. The following event numbers and errors are obtained for the charm and beauty contributions from the two-dimensional fit:

$$N_c = 53 \pm 12 \qquad\qquad N_b = 66 \pm 17.$$

5.1 Total Cross Section

The number of b and c events are used to compute the total cross sections in the kinematic region defined in table 3. The efficiencies and acceptances are derived from the Monte Carlo simulations. Values of

Charm	Cross section [pb]	Data/Theory
Data	$250 \pm 57 \pm 40$	
PYTHIA (direct)	242 (142)	1.0
CASCADE	253	1.0
FMNR	286^{+159}_{-59}	0.9
Beauty		
Data	$206 \pm 53 \pm 35$	
PYTHIA (direct)	57 (44)	3.6
CASCADE	56	3.7
FMNR	52^{+14}_{-9}	4.0

Table 4: *Measured $D^*\mu$ cross sections for charm and beauty production in the kinematic region defined in table 3. For the data the statistical and the systematic errors are given. The LO-ME+PS predictions (PYTHIA, CASCADE) and NLO calculations (FMNR) are also shown. The uncertainties of the FMNR results are obtained by varying the renormalisation and the factorisation scales simultaneously by factors of 0.5 and 2. The uncertainty due to a variation of the quark masses m_c by ± 0.2 GeV and m_b by ± 0.25 GeV is added quadratically. The last column shows the ratios of the measurement to the prediction.*

$$\sigma^c_{vis}(ep \to e\, D^*\mu X) = 250 \pm 57 \text{ (stat.)} \pm 40 \text{ (syst.) pb}$$

and of

$$\sigma^b_{vis}(ep \to e\, D^*\mu X) = 206 \pm 53 \text{ (stat.)} \pm 35 \text{ (syst.) pb}$$

are obtained for charm and beauty production, respectively. The measured cross sections are similar due to the definition of the visible kinematic region, which requires in particular a high momentum muon, suppressing central charm production. The results are compared with the pQCD predictions in table 4, where error estimates due to the uncertainty of the quark masses and the scales are given for the NLO calculations. In order to assess the influence of mass effects in the extraction of gluon densities used in the calculations, the default CTEQ5M sets have been replaced by the CTEQ5F sets [30]. The results are found to be compatible. The uncertainties for PYTHIA and CASCADE are found to be of similar size as those of the NLO calculations. The measured cross section for charm production agrees well with the LO-ME+PS models (PYTHIA and CASCADE) and the NLO prediction (FMNR). The measured beauty cross section exceeds the calculated cross sections. In other recent measurements of the beauty cross section in photoproduction at HERA [12, 15], based on the selection of high transverse momentum jets, ratios of measurement and FMNR based calculations between 1 and 3 are found. Note that the present analysis extends down to the production threshold for $b\bar{b}$, while the jet measurements have a threshold which is approximately 5 GeV higher in the $b\bar{b}$ centre-of-mass system.

The systematic uncertainties of the cross section measurement are evaluated by varying the Monte Carlo simulations. The dominant experimental errors come from the uncertainties in the track reconstruction efficiency (13%), the trigger efficiency (5%) and the width of the ΔM signal (3%). Smaller contributions are due to uncertainties in the determination of the background due to misidentified muons[5] (1%;1.5%) and in the fragmentation fractions (1%;1.5%). Model uncertainties are estimated using the CASCADE Monte Carlo generator instead of PYTHIA (3.5%) and either taking into account or omitting the resolved component in PYTHIA (3%;5%). Taking into account the uncertainties due to the contribution of D^* reflections (5%), the muon identification, the luminosity measurement and the D^* decay branching ratios, the total systematic errors for the charm and beauty cross sections are estimated to be 16% and 17%, respectively.

5.2 Differential Cross Sections for Charm and Beauty

Differential cross sections for $D^*\mu$ production in the visible kinematic region are evaluated as functions of variables characterising the D^* meson, the muon and the $D^*\mu$ system. In this section results are presented for the complete data set, which contains the contributions from charm and beauty (figures 4 and 5).

In order to compute the differential cross sections for the data, the numbers of events in bins of the chosen variable are determined by a fit to the ΔM distribution in each bin, as described in section 4.2. Here, no attempt is made to separate charm and beauty contributions. A correction for 'fake muons' is applied according to the Monte Carlo simulation. Since the fake muon fraction is different for charm and beauty, it is computed using the b fraction of 45% given by the measured cross sections (table 4).

The data are shown with the results of the PYTHIA and CASCADE Monte Carlo models and the LO and NLO FMNR calculations. In the theoretical models, the beauty and charm contributions are combined according to the measured total visible cross sections (table 4) and normalised to the sum of these cross sections, in order to facilitate a shape comparison. The error bands for the FMNR prediction are computed as for the total cross section (see caption of table 4). The measured differential cross sections are similarly normalised, which has the advantage that the systematic errors largely cancel and are negligible compared to the statistical errors.

Figure 4 shows the differential cross sections as a function of the transverse momentum and pseudorapidity of the D^* meson and the muon separately. Overall the QCD models describe the shapes of the measured distributions quite well, although there is a tendency for the measured $p_T(D^*)$ and $p_T(\mu)$ distributions to be softer than the calculations. A slight discrepancy is also present in the differential cross section as a function of the pseudorapidity of the muon (figure 4c) which shows a central dip due to the large muon momentum required.

Quantities derived from a combined measurement of the D^* and muon are shown in figure 5. In figures 5a and c, the differential cross sections as a function of $p_T(D^*\mu)$, which is defined as $p_T(D^*\mu) = |\vec{p}_T(D^*)+\vec{p}_T(\mu)|$, and $\Delta\Phi$ are compared with the LO and NLO FMNR predictions. The data show the expected deviations from the LO calculations due to higher order effects: the observed $p_T(D^*\mu)$ distribution is flatter and the $\Delta\Phi$ peak around 180° is broader than the LO computation. The data are in good agreement with the NLO calculation. In figures 5b and d, the same differential cross sections for $p_T(D^*\mu)$ and $\Delta\Phi$ are compared with PYTHIA and CASCADE which also give a good description of the data. Although different approaches are used

[5] Where two numbers are given the first applies to charm and the second to beauty.

in PYTHIA and CASCADE to compute the evolution of the partons from the proton and the hard interaction, the differences between the two simulations are smaller than the experimental errors.

Figures 5e and f show the invariant mass, $M(D^*\mu)$, and the rapidity[6], $\hat{y}(D^*\mu)$, of the D^* meson and the muon together with NLO FMNR, PYTHIA and CASCADE predictions. The invariant mass $M(D^*\mu)$ reflects the centre-of-mass energy of the quark pair and $\hat{y}(D^*\mu)$ is related to the ratio of the energies of the partons entering the hard interaction from the proton and the photon. Both differential cross sections are adequately described by all model calculations.

5.3 Results for a Charm Dominated 'Quark Antiquark Tag' Sample

The cross sections in the previous section refer to the complete data set including events from region III in which both D^* and muon originate from the same b quark. Since this leads to a dilution of the correlation of quantities characterising the quark pair and the measured $D^*\mu$ pair, results for a smaller sample are given here, where both the heavy quark and the antiquark are tagged by either a D^* or a muon ('quark antiquark tag'). This is possible in correlation region IV ($\Delta\Phi > 90°$ and $Q(D^*) \neq Q(\mu)$). This region (see figure 1) is dominated by $c\bar{c}$ pairs: the $b\bar{b}$ contribution is 18% according to the two-dimensional fit. Due to migrations from correlation region III, approximately half of the $b\bar{b}$ contribution is due to $b \to D^*\mu$ events in which the $D^*\mu$ pair comes from the same b quark (according to the PYTHIA simulation). A visible cross section of $\sigma_{2q} = 263 \pm 48 \pm 36$ pb is measured[7] after subtracting this fraction, while 264^{+148}_{-50} pb is expected from the FMNR calculations.

In this data sample, the correlation of kinematic quantities reconstructed using the D^* meson and the muon to those of the quark pairs is good for x_g and $\hat{y}(D^*\mu)$, while it is weaker for $p_T(D^*\mu)$. Here x_g is the fraction of the proton energy carried by the gluon in the hard interaction, which is approximated by $x_g^{obs} = (M(D^*\mu))^2/y\,s$. The normalised differential cross section for $x_g^{obs}(D^*\mu)$ is shown in figure 6a. All QCD calculations (FMNR to LO and NLO, PYTHIA and CASCADE) give a reasonable description of the data. Figure 6b and c show the $p_T(D^*\mu)$ and $\hat{y}(D^*\mu)$ distributions of the $D^*\mu$ pair, respectively, with the same model calculations. The LO FMNR prediction for $p_T(D^*\mu)$ is again too soft, as observed for the total sample (figure 5a), while the NLO FMNR prediction fits the data well. Although this sample should be sensitive to any transverse momentum of the incoming gluon, the differences between PYTHIA (collinear factorisation) and CASCADE (k_t factorisation) are small in the kinematic region studied.

Conclusion

A measurement of $c\bar{c}$ and $b\bar{b}$ photoproduction cross sections using the H1 detector at HERA has been presented. For the majority of events both heavy quarks are tagged using a D^* meson and a

[6] $\hat{y} = 1/2\,\ln{(E+p_z)/(E-p_z)}$, where E and p_z are the energy and the z-component of the momentum of the $D^*\mu$ pair.

[7] The index '$2q$' is used for the cross sections in this section to distinguish them from those in the previous section.

muon as signatures. The separation of the charm and beauty contributions is possible due to the different correlations between the charges and angles between the D^* meson and the muon. The measured total cross section for charm in the visible kinematic region is in agreement with the NLO QCD prediction, while the beauty cross section is higher than predicted. The kinematic region of the latter is characterised by lower $b\bar{b}$ centre-of-mass energies than in most previous analyses, which require high momentum jets. Comparisons of the shapes of the measured differential distributions with QCD calculations including higher order effects show general agreement. Effects beyond the LO approximation are directly observed. In the kinematic region studied, effects due to k_t factorisation, as implemented in CASCADE, are found to be small compared to the experimental errors.

Acknowledgements

We are grateful to the HERA machine group whose outstanding efforts have made this experiment possible. We thank the engineers and technicians for their work in constructing and maintaining the H1 detector, our funding agencies for financial support, the DESY technical staff for continual assistance and the DESY directorate for support and for the hospitality which they extend to the non DESY members of the collaboration.

References

[1] A. Aktas *et al.* [H1 Coll.], Eur. Phys. J. C **38** (2005) 447, [hep-ex/0408149]

[2] C. Adloff *et al.* [H1 Coll.], Phys. Lett. B **528** (2002) 199, [hep-ex/0108039]

[3] C. Adloff *et al.* [H1 Coll.], Nucl. Phys. B **545** (1999) 21, [hep-ex/9812023]

[4] S. Aid *et al.* [H1 Coll.], Nucl. Phys. B **472** (1996) 32, [hep-ex/9604005]

[5] S. Chekanov *et al.* [ZEUS Coll.], Phys. Rev. D **69** (2004) 012004, [hep-ex/0308068]

[6] S. Chekanov *et al.* [ZEUS Coll.], Phys. Lett. B **565** (2003) 87, [hep-ex/0302025]

[7] J. Breitweg *et al.* [ZEUS Coll.], Phys. Lett. B **481** (2000) 213, [hep-ex/0003018]

[8] J. Breitweg *et al.* [ZEUS Coll.], Eur. Phys. J. C **12** (2000) 35, [hep-ex/9908012]

[9] J. Breitweg *et al.* [ZEUS Coll.], Eur. Phys. J. C **6** (1999) 67, [hep-ex/9807008]

[10] J. Breitweg *et al.* [ZEUS Coll.], Phys. Lett. B **407** (1997) 402, [hep-ex/9706009]

[11] J. Breitweg *et al.* [ZEUS Coll.], Phys. Lett. B **401** (1997) 192, [hep-ex/9704011]

[12] A. Aktas *et al.* [H1 Coll.], DESY-05-004, submitted to Eur. Phys. J. C, [hep-ex/0502010]

[13] A. Aktas *et al.* [H1 Coll.], DESY-04-209, submitted to Eur. Phys. J. C, [hep-ex/0411046]

[14] C. Adloff *et al.* [H1 Coll.], Phys. Lett. B **467** (1999) 156; erratum *ibid* B **518** (2001) 331, [hep-ex/9909029]

[15] S. Chekanov *et al.* [ZEUS Coll.], Phys. Rev. D **70** (2004) 012008, [hep-ex/0312057]

[16] S. Chekanov *et al.* [ZEUS Coll.], Phys. Lett. B **599** (2004) 173, [hep-ex/0405069]

[17] J. Breitweg *et al.* [ZEUS Coll.], Eur. Phys. J. C **18** (2001) 625, [hep-ex/0011081]

[18] T. Sjöstrand, Comput. Phys. Commun. **82** (1994) 74;
T. Sjöstrand et al., Comput. Phys. Commun. **135** (2001) 238, [hep-ph/0010017]

[19] H. Jung and G. P. Salam, Eur. Phys. J. C **19** (2001) 351, [hep-ph/0012143];
H. Jung, Comput. Phys. Commun. **143** (2002) 100, [hep-ph/0109102];
M. Hansson, H. Jung, proceedings of DIS 2003, St. Petersburg, Russia, 23-27 Apr 2003, [hep-ph/0309009]

[20] V.N. Gribov and L.N. Lipatov, Yad. Fiz. **15** (1972) 781[Sov. J. Nucl. Phys. **15** (1972) 438];
G. Altarelli and G. Parisi, Nucl. Phys. B **126** (1977) 298;
Y.L. Dokshitzer, Sov. Phys. JETP **46** (1977) 641 [Zh. Eksp. Teor. Fiz. **73** (1977) 1216]

[21] E. Norrbin and T. Sjöstrand, Eur. Phys. J. C **17** (2000) 137, [hep-ph/0005110]

[22] M. Ciafaloni, Nucl. Phys. B **296** (1988) 49;
S. Catani, F. Fiorani and G. Marchesini, Phys. Lett. B **234** (1990) 339

[23] C. Peterson, D. Schlatter, I. Schmitt and P. M. Zerwas, Phys. Rev. D **27** (1983) 105

[24] R. Brun et al., CERN-DD/EE/84-1

[25] S. Frixione, P. Nason and G. Ridolfi, Nucl. Phys. B **454** (1995) 3, [hep-ph/9506226]

[26] S. Frixione, M. L. Mangano, P. Nason and G. Ridolfi, Phys. Lett. B **348** (1995) 633, [hep-ph/9412348]

[27] K. Ackerstaff *et al.* [OPAL Coll.], Eur. Phys. J. C **1** (1998) 439, [hep-ex/9708021]

[28] K. Hagiwara *et al.* [Particle Data Group Coll.], Phys. Rev. D **66** (2002) 010001

[29] P. Nason and C. Oleari, Nucl. Phys. B **565** (2000) 245, [hep-ph/9903541]

[30] H. L. Lai *et al.* [CTEQ Coll.], Eur. Phys. J. C **12** (2000) 375, [hep-ph/9903282]

[31] M. Glück, E. Reya and A. Vogt, Phys. Rev. D **45** (1992) 3986; Phys. Rev. D **46** (1992) 1973

[32] I. Abt *et al.* [H1 Coll.], Nucl. Instrum. Meth. A **386** (1997) 310 and 348

[33] R. D. Appuhn *et al.* [H1 SPACAL Coll.], Nucl. Instrum. Meth. A **386** (1997) 397

[34] J. Wagner, Dissertation, Univ. Hamburg, DESY-THESIS-2004-022, available at http://www-h1.desy.de/publications/theses_list.html

[35] A. Blondel and F. Jacquet, Proc. *Study of an ep Facility for Europe* (Ed. U. Amaldi), DESY 79/48 (1979) 391

[36] G. J. Feldman *et al.*, Phys. Rev. Lett. **38** (1977) 1313

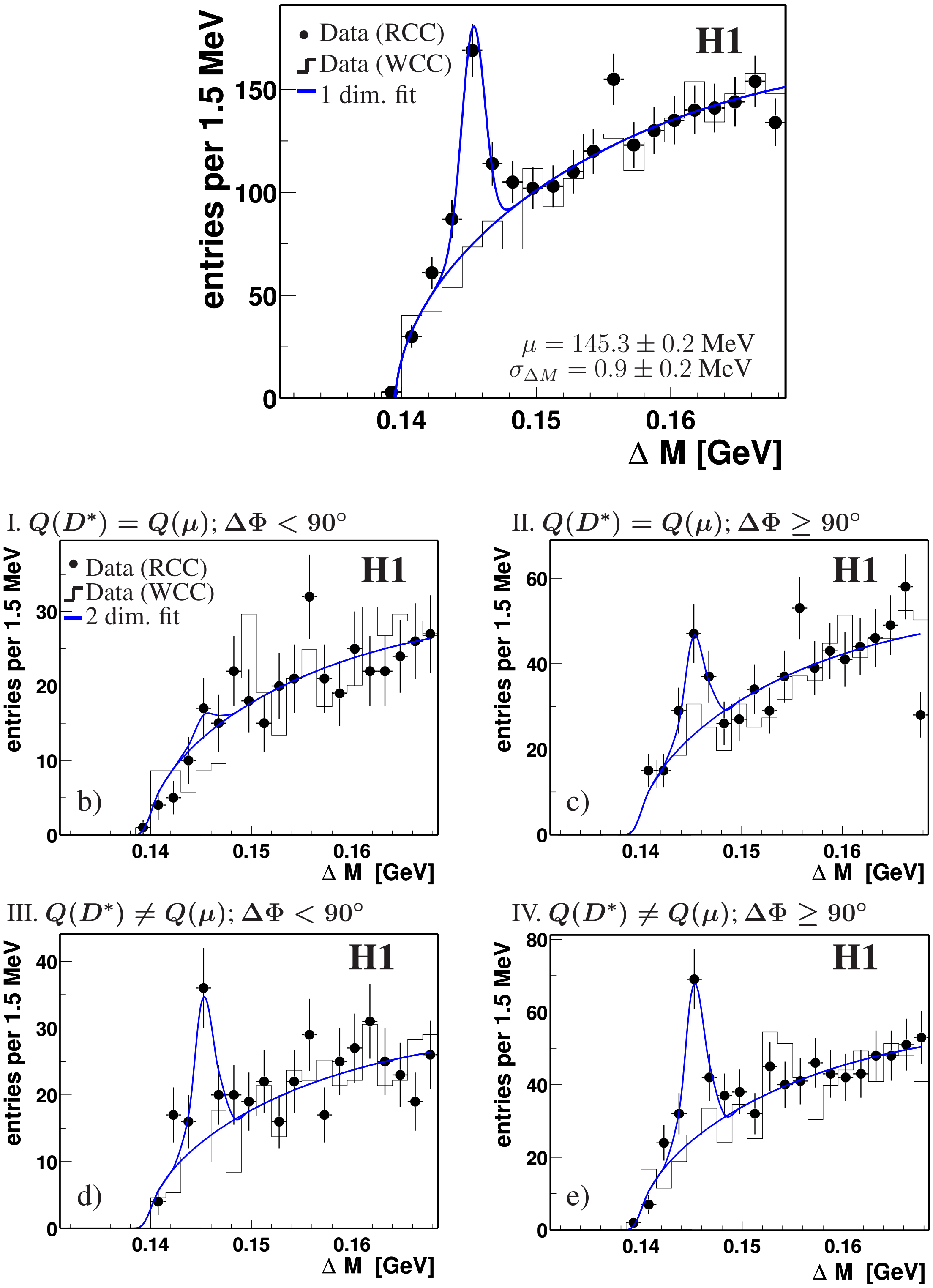

Figure 2: *a) Distribution of the mass difference $\Delta M = m_{K\pi\pi_s} - m_{K\pi}$ for the total data sample. In b)-e) ΔM is shown in the four correlation regions, given by the relative charges of the D^* and the muon and the azimuthal angle $\Delta\Phi$ between them. The points represent the data (right charge combinations, RCC), the histogram indicates the observed wrong charge combinations (WCC) which are also used to fit the background. The solid lines in a) are the result of a one-dimensional fit, which gives the peak position μ and the peak width $\sigma_{\Delta M}$. The solid lines in b)-e) are results of a two-dimensional fit (see text).*

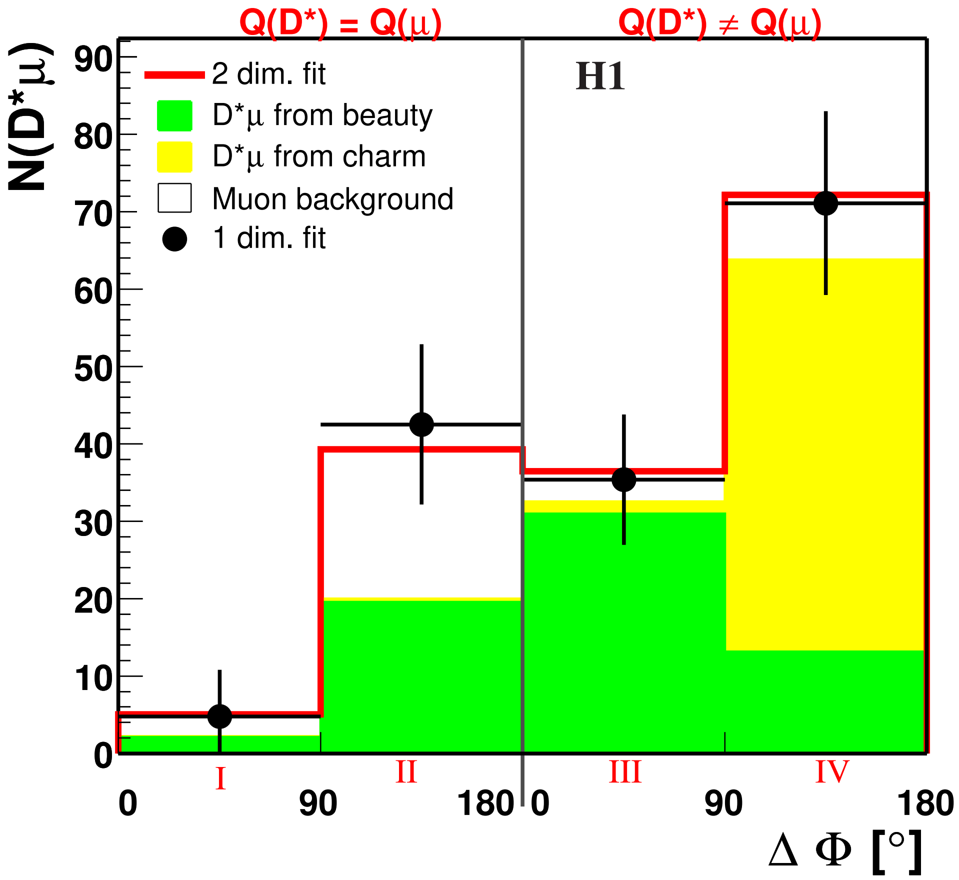

Figure 3: *Population of the four correlation regions I-IV obtained from the simultaneous likelihood fit in all correlation regions (two-dimensional fit, histogram). The resulting decomposition into charm and beauty contributions and the muon background is also shown. In all correlation regions the muon background is dominated by charm initiated events. The points with error bars are the results of one-dimensional fits of the* ΔM *distributions in each correlation region.*

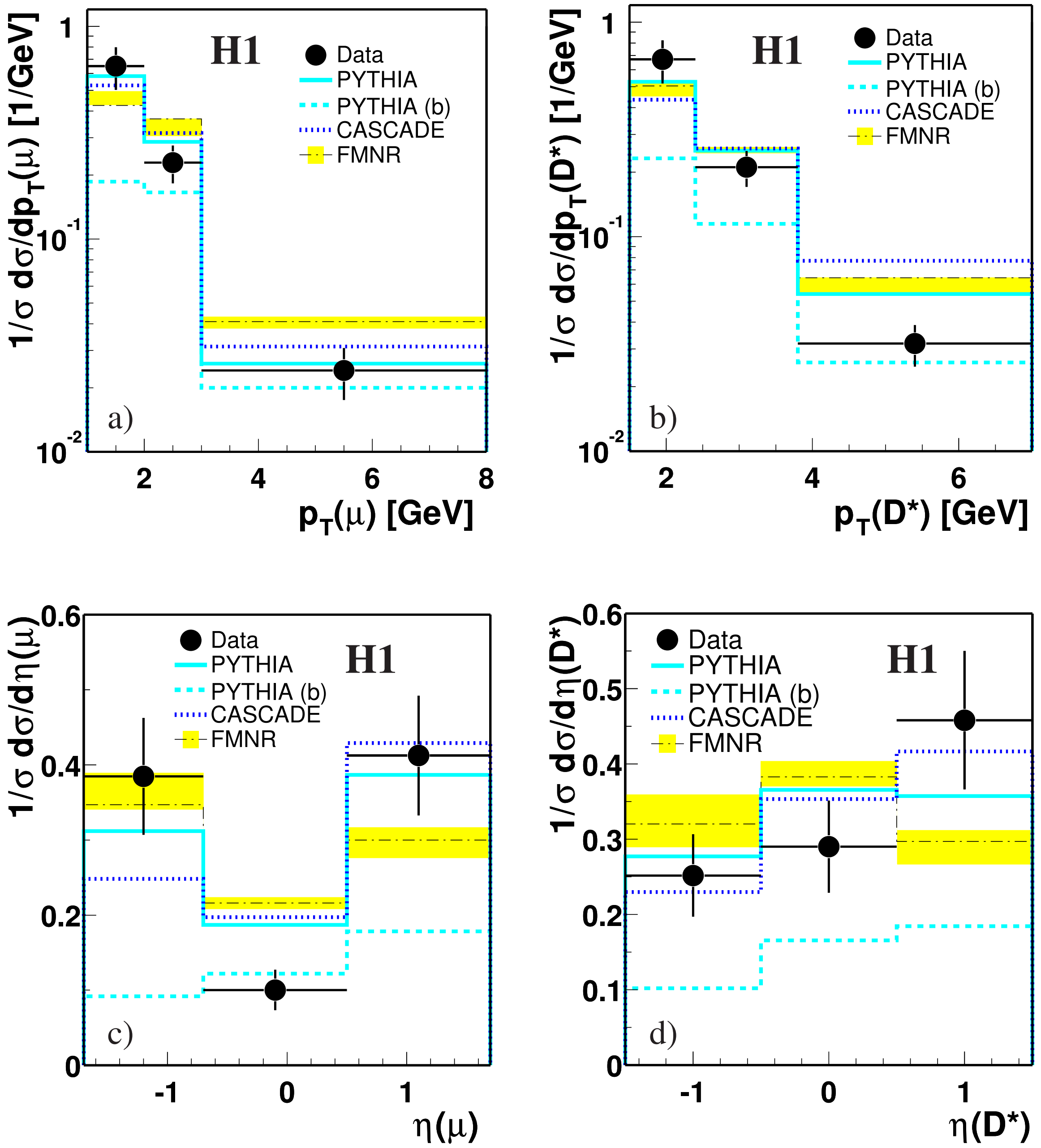

Figure 4: *Normalised differential $D^*\mu$ cross sections as functions of the transverse momenta and the pseudorapidities of muons (a,c) and D^* mesons (b,d). The data (points) are compared with the prediction of the NLO calculation FMNR and the LO-ME+PS QCD models PYTHIA and CASCADE. A beauty fraction of 45% as obtained from the measured cross sections is used in the calculations. The error bands for FMNR are obtained as described in table 4. The PYTHIA b quark contribution is indicated separately. The experimental systematic uncertainties for the normalised distributions are negligible compared to the statistical errors.*

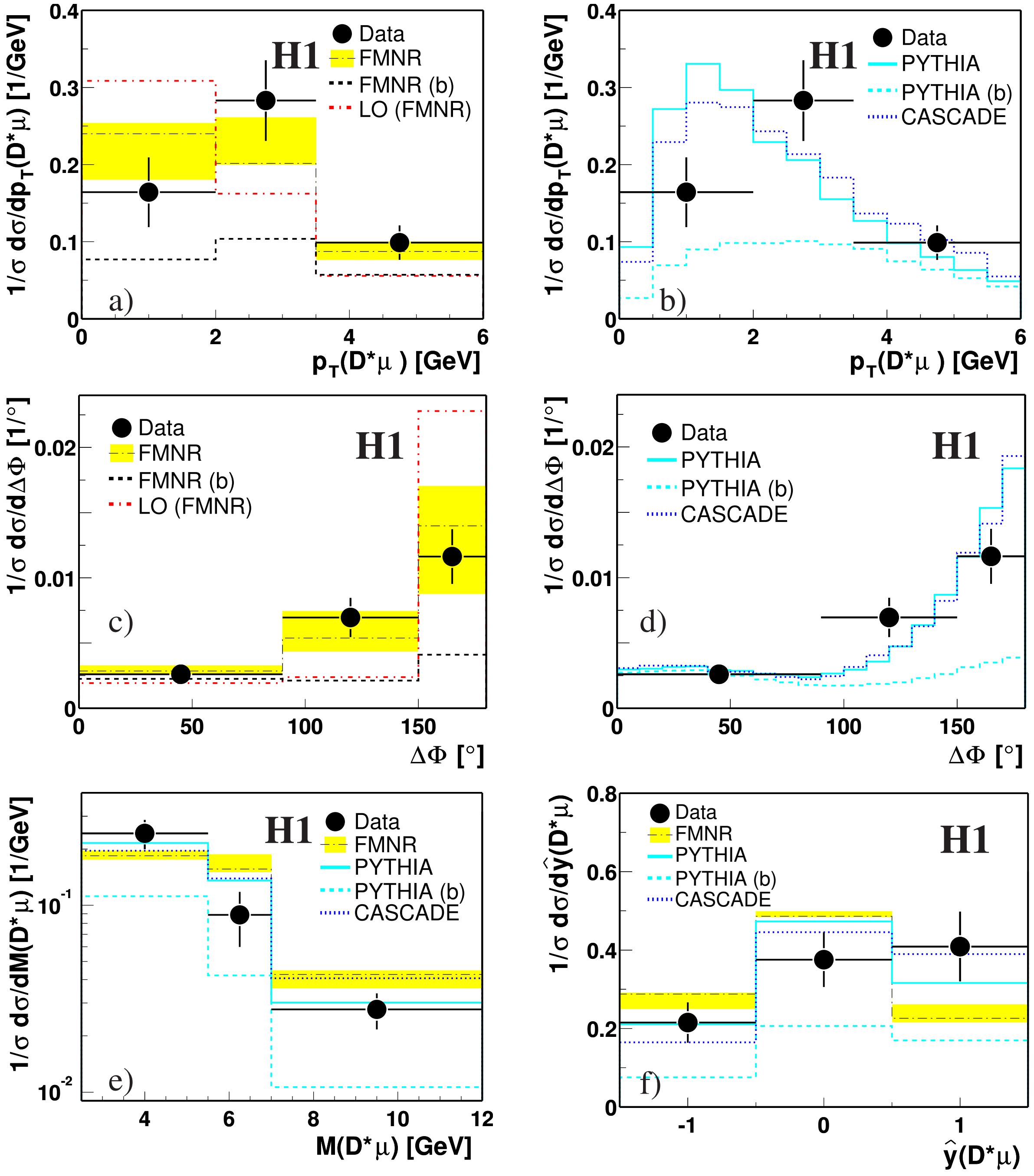

Figure 5: *Normalised differential $D^*\mu$ cross sections for a,b) the transverse momenta $p_T(D^*\mu)$, c,d) the azimuthal angle difference $\Delta\Phi$, e) the invariant mass $M(D^*\mu)$ and f) the rapidity $\hat{y}(D^*\mu)$ of the $D^*\mu$-pairs. The data are compared to the prediction of the LO and NLO calculations FMNR (a,c,e,f) and to the Monte Carlo models PYTHIA and CASCADE (b,d,e,f). The error bands for FMNR are obtained as described in table 4. A beauty fraction of 45% as obtained from the measured cross sections is used in the calculations. The FMNR (a,c) and PYTHIA (b,d,e,f) b quark contributions are indicated separately. The experimental systematic uncertainties for the normalised distributions are negligible compared to the statistical errors.*

QUARK ANTIQUARK TAG

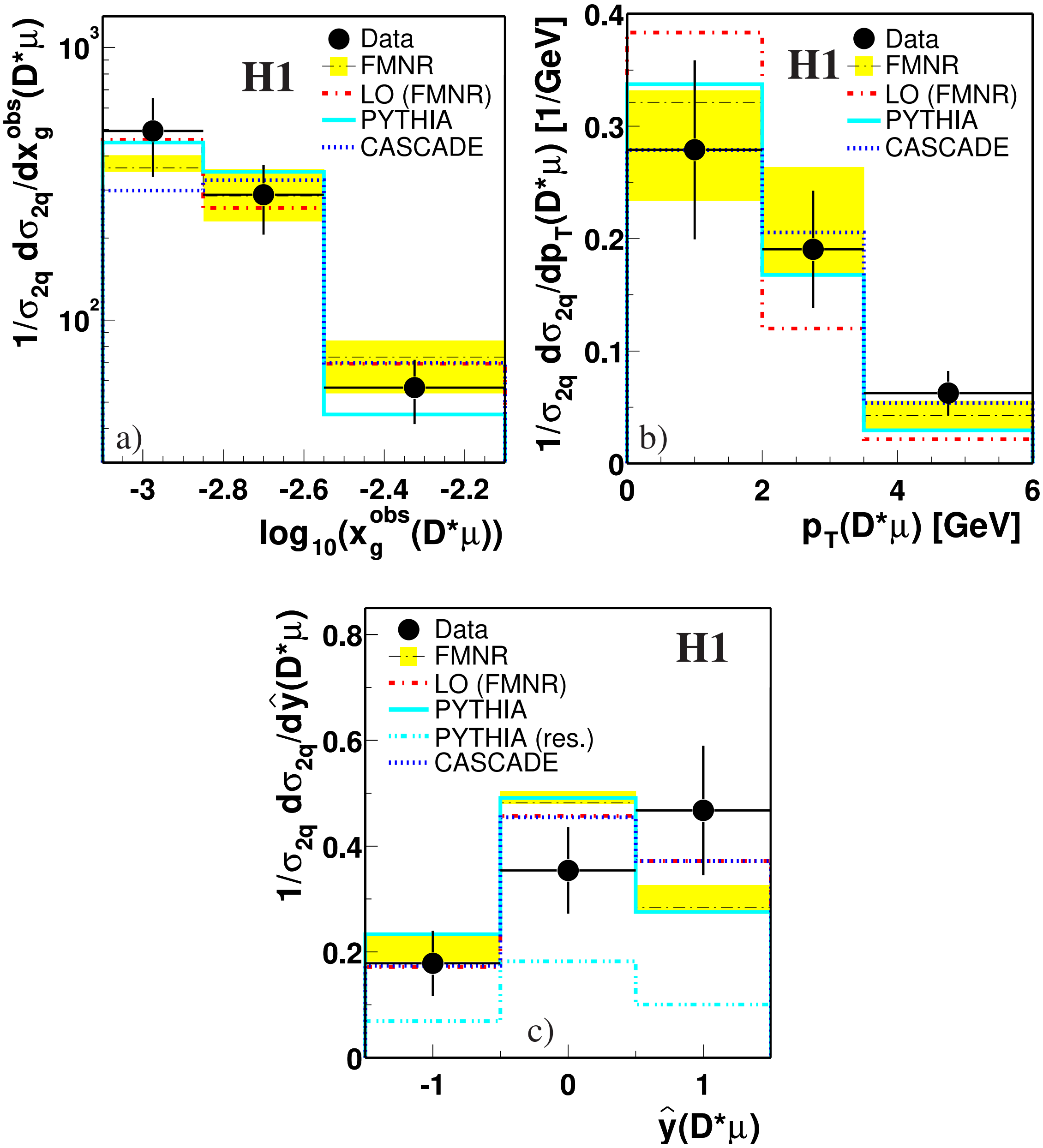

Figure 6: *Normalised differential $D^*\mu$ cross sections for a 'quark antiquark tag', charm dominated sample (approximately 10% $b\bar{b}$ quark contamination), where the D^* and the μ originate from different quarks. The data and predictions of the LO and NLO calculation FMNR and of the Monte Carlo generators PYTHIA and CASCADE are shown. The error bands for FMNR are obtained as described in table 4. In c) the resolved excitation component of PYTHIA is indicated separately. The experimental systematic uncertainties for the normalised distributions are negligible compared to the statistical errors.*